

New Bag of Deep Visual Words based features to classify chest x-ray images for COVID-19 diagnosis

Chiranjibi Sitaula*, Sunil Aryal

School of Information Technology, Deakin University, Geelong, 3216, Victoria, Australia

Abstract

Because the infection by Severe Acute Respiratory Syndrome Coronavirus 2 (COVID-19) causes the pneumonia-like effect in the lungs, the examination of chest x-rays can help to diagnose the diseases. For automatic analysis of images, they are represented in machines by a set of semantic features. Deep Learning (DL) models are widely used to extract features from images. General deep features may not be appropriate to represent chest x-rays as they have a few semantic regions. Though the Bag of Visual Words (BoVW) based features are shown to be more appropriate for x-ray type of images, existing BoVW features may not capture enough information to differentiate COVID-19 infection from other pneumonia-related infections. In this paper, we propose a new BoVW method over deep features, called Bag of Deep Visual Words (BoDVW), by removing the feature map normalization step and adding deep features normalization step on the raw feature maps. This helps to preserve the semantics of each feature map that may have important clues to differentiate COVID-19 from pneumonia. We evaluate the effectiveness of our proposed BoDVW features in chest x-rays classification using Support Vector Machine (SVM) to diagnose COVID-19. Our results on a publicly available COVID-19 x-ray dataset reveal that our features produce stable and prominent classification accuracy, particularly differentiating COVID-19 infection from other pneumonia, in shorter computation time compared to the state-of-the-art methods. Thus, our method

*Corresponding Author

Email address: csitaul@deakin.edu.au (Chiranjibi Sitaula)

could be a very useful tool for quick diagnosis of COVID-19 patients on a large scale.

Keywords: COVID-19, SARS-CoV-2, Chest X-Ray, Bag of Visual Words (BoVW), Deep Features, Bag of Deep Visual Words (BoDVW)

1. Introduction

The disease caused by Severe Acute Respiratory Syndrome Coronavirus 2 (SARS-CoV-2) [22, 26, 36], commonly known as COVID-19, was originated in Wuhan city of China in late 2019 [38]. At first, it was believed that the coronavirus was transmitted from Bat to humans in China. Now, the virus has been transmitting from human to human in all around the world [16, 11, 3]. It has spread over 200 countries in the world at present and become pandemic that has killed over 298,083 people¹ and 98 people in Australia alone², so far. While analyzing the effect of the SARS-CoV-2 virus in the human body, it has been known that it causes the pneumonia-like effect in the lungs. Thus, the study of chest x-ray images could be an alternative to a swab test for early quick diagnosis of the COVID-19. An automated chest x-ray image analysis tool can be very useful to health practitioners for mass screening of people quickly.

For automatic analysis of images using algorithms, they are represented in machines by a set of semantic features. The large artificial neural network, also known as Deep Learning (DL), based models are widely used to extract features from images and shown to work well in various types of images [43, 39, 40, 42, 13, 30]. A few research studies have used DL models to analyze chest x-ray images for coronavirus diagnosis too. For instance, two recent works [27, 30] include the fine-tuning approach of transfer learning on pre-trained DL models such as AlexNet [20], ResNet-18 [14], GoogleNet [46], etc. These methods require a massive amount of data to train DL models in addition

¹<https://www.worldometers.info/coronavirus/> (accessed date: 14/05/2020)

²<https://www.health.gov.au/news/health-alerts/novel-coronavirus-2019-ncov-health-alert/coronavirus-covid-19-current-situation-and-case-numbers>. (accessed date: 14/05/2020)

to extensive hyperparameter tuning. However, chest x-ray images related to COVID-19 are very limited. Thus, working on a limited amount of data is always a challenging problem in fine-tuning tasks. Similarly, unlike in other types of images, existing features extraction methods such as GAP (global average pooling) features achieved from pre-trained models may not provide accurate representation for chest x-ray images because of their sparsity (i.e., having fewer semantic regions). Also, x-ray scans of lungs infected by COVID-19 and other pneumonia look similar (i.e., there is a high degree of inter-class similarities).

Bag of Visual Words (BoVW) based features are shown to be more appropriate in images with the characters discussed above (sparsity and high inter-class similarity). They consider visual patterns/clues (known as visual words) in each image in the collection, thereby capturing sparse interesting regions in the image which are useful in dealing with the inter-class similarity problem to some degree. BoVW based feature extraction approach is popular not only in traditional computer vision-based methods such as Scale Invariant Features Transform (SIFT) [28] but also in DL based methods due to its ability to capture semantic information extracted from the feature map of pre-trained DL models. The Bag of Deep Visual Words (BoDVW) features designed for one domain (e.g., satellite images) may not work exactly for another domain (e.g., chest x-ray images) due to the varying nature of the images. For example, the bag of Deep Convolutional Features (DCF-BoVW) [49] designed for satellite images may not work exactly for health images such as chest x-rays. This is because of the fact that satellite image contains numerous semantic regions scattered in the image (dense) and thus, DCF-BoVW could capture enough semantic regions of such images. However, the chest x-ray image contains fewer semantic regions (sparse), which may not be captured accurately by DCF-BoVW.

In this paper, we propose a new BoDVW based features to represent chest x-ray images. Our method eliminates some of the intermediate steps present in DCF-BoVW [49] and adds new steps because of the nature of chest x-ray images. For this, we adopt the following steps. Initially, we extract the raw feature map from the mid-level (4^{th} pooling layer) of the VGG16 pre-trained

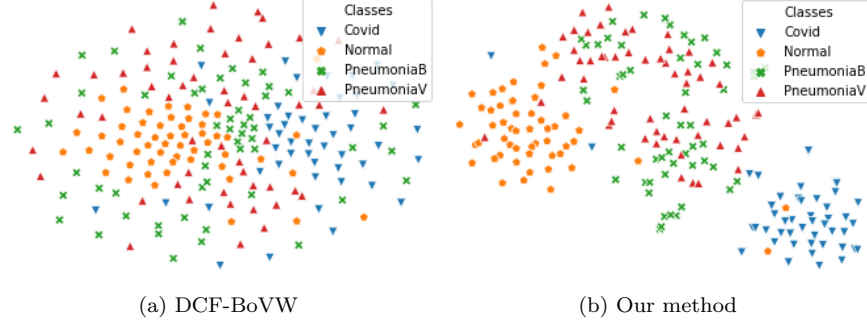


Figure 1: Scatter plot of two dimensional projection of features produced by DCF-BoVW and our proposed method based on t-SNE visualization in the COVID-19 dataset [8].

DL model [37] for each input image. Then, we perform L2-normalisation to each deep features vector over the depth of the feature map. Using the training set, we design a codebook or dictionary over such deep features extracted from all the training images. Then, based on such a codebook, we achieve our proposed features using a bag of visual words method for each input image. Such features based on the bag of visual words method is, finally, normalized by L2-norm, which acts as the final representation of the input image. Because our final features are based on patterns extracted from mid-level features from training images, they capture the more discriminating clues of sparse chest x-ray images. The comparison of two-dimensional projections of features produced by DCF-BoVW and our proposed method on the COVID-19 image dataset [8] based on the t-SNE visualization [29] is shown in Fig. 1. It reveals that our features offer higher separability between COVID, Normal, and two Pneumonia classes though there is some overlap of bacterial and viral pneumonia (PneumoniaB and PneumoniaV).

The main **contributions** in our work are as follows:

- (a) We propose to use the improved version of a bag of visual words method over deep features to work for the chest x-ray images representation. We used deep features extracted from the fourth pooling layers (p_4) of the VGG16 model to achieve our proposed features for chest x-ray images. To

design a codebook from deep features, we used unsupervised clustering with the simple k -means algorithm.

- (b) We evaluate our features against the existing BoVW features (DCF-BoVW) and deep features achieved using *GAP* (global average pooling) operation from various pre-trained DL models in the chest x-ray classification task using the Support Vector Machine classifier. We also compare our method with Loey et al. (2020)’s classification model used in the same COVID-19 dataset using their exact train-test split. The results show that our method produces stable and state-of-the-art classification performance, particularly differentiating COVID cases from others. Also, our feature size is the smallest compared to all the contenders making our method faster than others.

The remainder of the paper is organized as follows. In Sec. 2, we review some of the recent related works on chest x-ray image representation and classification. Similarly, we discuss our proposed method in Sec. 3 in a step-wise manner. Furthermore, Sec. 4 details the experimental setup, comparison, and ablative study associated with it. Finally, Sec. 5 concludes our paper with potential directions for future research.

2. Related works

Deep Learning (DL) has been a breakthrough in image processing producing significant performance improvement in tasks such as classification and object detection. A DL model is a larger artificial neural network (ANN), which is inspired by the structure and function of the brain. If we design our DL model from scratch and train it, it is called a user-defined DL model. Similarly, if we use existing deep learning architectures pre-trained on large datasets, such as ImageNet [10] or Places [50], they are called pre-trained DL model. The features extracted from intermediate layers of DL models either user-defined or pre-trained provide rich semantic features to represent images that result in significantly better task-specific performance than traditional computer vision

methods such as Scale Invariant Feature Transform (SIFT) [28], Generalized Search Tree (GIST)-color [32], Generalized Search Trees (GIST) [31], Histogram of Gradient (HOG) [9], Spatial Pyramid Matching (SPM) [23], etc.

Thus, in this section, we review some of the recent works in chest x-ray classification using DL models [44, 18, 2, 48, 7, 27, 35, 30]. We categorize them into two groups: 2.1 standalone deep learning algorithms and 2.2 ensemble learning algorithms

2.1. Standalone deep learning algorithms

Stephen et al. [44] presented a model to detect pneumonia using DL and machine learning approach. They trained a Convolutional Neural Network (CNN) from scratch using a collection of chest x-ray images. Similarly, Islam et al [18] introduced a Compressed Sensing (CS) based DL model for automatic classification of chest x-rays for pneumonia. Similarly, Ayan et al. [2] used DL models on chest x-ray images for early diagnosis of pneumonia. They used Xception [5] and VGG16 [37] pre-trained models. Their results unveil that the VGG16 model outperforms the Xception model in terms of classification accuracy. This strengthens the efficacy VGG16 model for such an image representation task. Thus, the use of a pre-trained model became widespread in the representation and classification task of such images. For example, Varshni et al. [48] leveraged several pre-trained models such as VGG16 [37], Xception [5], ResNet50 [14], DenseNet-121 [17], and DenseNet169 [17] individually as the features extractors and trained four classifiers separately using SVM [15], Random Forest [4], k-nearest neighbors [1], and Naïve Bayes [24] for the classification purpose. Furthermore, Loey et al. [27] used Generative Adversarial Networks (GAN) [12] and transfer learning approach on AlexNet [20], GoogleNet [46], and ResNet-18 [14] to classify the COVID-19 images dataset where x-ray images belong to one of the four categories - Covid, Normal, Bacterial pneumonia (PneumoniaB), and Viral Pneumonia (PneumoniaV). In their method, GAN was used to augment the chest x-ray images to avoid overfitting in the training phase. Recently, Sitaula et al. [41] employed the attention module on top of VGG-

16 model for the chest x-ray images classification. Their method outperforms several state-of-the-art methods such image analysis.

2.2. Ensemble learning algorithms

Ensemble learning methods have also been used in chest x-ray image representation and classification where different types of features are combined for better discrimination images. Zhou et al. [51] proposed an ensemble learning approach of multiple artificial neural networks (ANNs) for the lung cancer cell identification tasks. Sasaki et al. [35] designed an ensemble learning approach using DL on chest x-ray images. In their method, they performed several filtering and pre-processing operations on images and then ensembled using DL for the detection of abnormality in chest x-ray images. Similarly, Li et al. [25] utilized more than two CNNs to reduce the false positive on lungs nodules of chest x-ray images. Islam et al. [18] designed an ensemble method to aggregate different pre-trained DL models for abnormality detection in lung images. Chouhan et al. [7] introduced a model, where the outputs of five pre-trained models (AlexNet, DenseNet-121, ResNet18, Inception-V3, GoogleNet) were ensembled for the detection of pneumonia using a transfer learning approach. This helps to learn multiple types of information achieved from various pre-trained DL models to bolster the classification performance. Nevertheless, ensemble learning algorithms are arduous for which we need to be vigilant in hyperparameter tuning in addition to the overfitting problem.

Most existing methods in the literature need a huge amount of data for fine-tuning DL models and most of them extract high-level features, which may not be sufficient for chest x-ray images. Chest x-ray images require mid-level features that are neither more generic nor more specific. In the next section, we introduce our proposed approach to extract such mid-level features.

3. Proposed method

The mid-level features of chest x-ray images can be achieved from the feature maps extracted from the intermediate layers of pre-trained models using a bag of

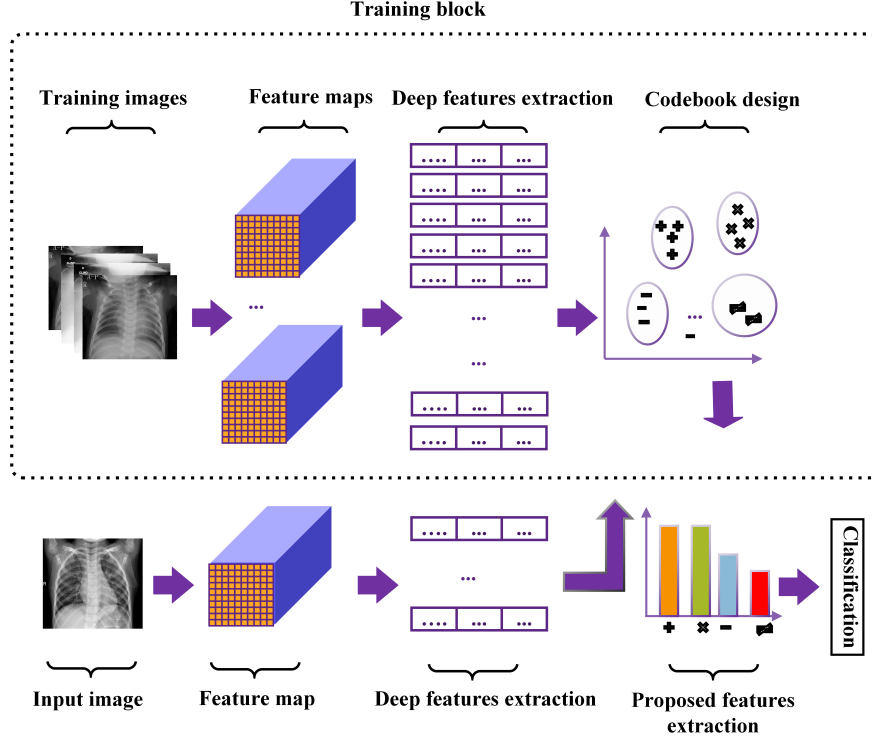


Figure 2: Pipeline of the proposed method. Based on the codebook or dictionary achieved from training block, the proposed features vector is extracted for each input image using the bag of visual features approach.

visual words (BoVW) method. Since chest x-ray images are sparse (having few semantic regions), an existing bag of visual words method that has been applied to represent other images (e.g., satellite images) may not work accurately in this domain. To this end, we propose an improved version of a bag of visual words method on deep features to represent chest x-ray images more accurately. In this section, we discuss the steps involved in our proposed feature extraction method. There are three main steps in our method: deep features extraction (Sec. 3.1), unsupervised codebook (dictionary) design (Sec. 3.2), and proposed features extraction (Sec. 3.3). The overall pipeline of the proposed method is shown in Fig. 2.



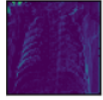
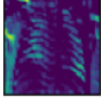
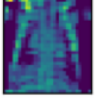
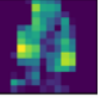



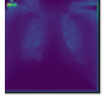
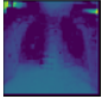
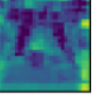




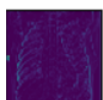
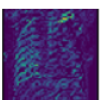
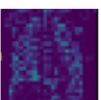
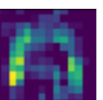



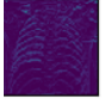
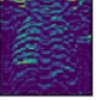
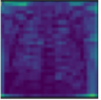


Category	Input image		p_1	p_2	p_3	p_4	p_5
PneumoniaB							
Covid							
Normal							
PneumoniaV							

Figure 3: Feature maps of an input image from each of the four categories in the COVID-19 dataset extracted from the five pooling layers of VGG16. p_i ($i = 1, 2, \dots, 5$) represents the i^{th} pooling layer.

3.1. Deep features extraction

At first, we extract the deep features from the feature map of the 4th pooling (p_4) layer from VGG16 [37], which is a deep learning model pre-trained on ImageNet [10]. We believe that 4th layer of such a model has a higher level of discriminability than other layers as seen in Fig. 3. The detailed discussion about the efficacy of the 4th pooling layer is also presented in Sec. 4.4. Furthermore, we use the VGG16 model due to its simple and prominent features extraction capability in various types of image representation tasks [43, 21, 13]. The size of the features map from the p_4 layer of the VGG16 model is 3-D shape having $H = 14$ (height), $W = 14$ width, and $L = 512$ (length). From each feature map, we achieve 14×14 number of features, each of size 512. Then, each features vector is L2-normalized. This normalization helps to preserve the separability

of deep features of images [13]. Let us say that an input image yields feature map with $14 \times 14 = 196$ number of features vectors that are represented by $x_0, x_1, x_2, \dots, x_{256}$. Each features vector x_i is of 512-D size (i.e., $|x_i| = 512$), which is then normalized by L2-norm as seen in Eq. (1).

$$x'_i = \frac{x_i}{||x_i||_2 + \epsilon} \quad (1)$$

In Eq. (1), the features vector x'_i represents the i^{th} normalized deep features vector extracted from the corresponding feature map. While achieving such features vector, we add $\epsilon = 0.00000008$ with denominator to avoid divide by zero exception because the feature map obtained for chest x-ray images is sparse and it is more likely to encounter with divide by zero exception in most cases.

3.2. Unsupervised dictionary (codebook) design

We used deep features (extracted from the VGG16 model as discussed above in Sec. 3.1) of all training images to design a dictionary or codebook. Each image provides $\{x'_i\}_{i=1}^{196}$ deep features and let's say there are m training images. Thus, the total number of deep features to design our codebook is $196 \times m$. To design the codebook or dictionary, we utilize a simple, yet popular unsupervised clustering algorithm, k -means, that groups deep features having similar patterns into clusters. Given a parameter k , k -means provide k groups or clusters ($\{c_1, c_2, \dots, c_k\}$) of deep features where deep features in each group are similar (i.e., they capture similar patterns of images). We use such k cluster centroids as a dictionary or codebook of deep visual words which is used to extract features for each input image.

3.3. Proposed features extraction

To extract features of each input image y , we first follow step 3.1 to achieve 256 normalized deep features of y and then, design a histogram based on the dictionary defined in step 3.2. The size of histogram is k (the dictionary size) where each code (cluster centroid) in the dictionary c_j has a weight w_j . All 256 deep features of y are assigned to their nearest centroids. The weight w_j is the

number of deep features assigned to the cluster c_j . In other words, histogram is a bag of visual words (centroids) where weights are their frequencies. The resulting features of y is a k -D vector $\{w_1, w_2, \dots, w_k\}$. The extracted bag of visual words features vector is, finally, normalized as in Eq. (1), which acts as our proposed features of the corresponding input image.

3.4. Difference between our BoVW and DCF-BoVW features

The main differences between our BoVW and DCF-BoVW features are explained in three different aspects.

Firstly, the L1-normalisation used by the DCF-BoVW method is more suitable for dense images such as satellite images. However, since the chest x-ray images are sparse in nature itself, such normalization becomes counterproductive as it masks some discriminating clues. Thus, we eliminate this normalization in our method due to the nature of chest x-ray images.

Secondly, we apply L2-normalisation to the deep features extracted from the unnormalized feature maps to exploit the property of cosine similarity in the k -means clustering. Note that Euclidean distance on the L2-normalised feature is equivalent to using cosine distance. The directions of deep features are more important than their lengths to group vectors with similar patterns into clusters to define our codebook. This will help us to detect sparse patterns in images which can be useful in discriminating abnormalities in x-ray images.

Table 1: Dataset description.

Classes	Total
Covid	69
Normal	79
PneumoniaB	79
PneumoniaV	79
Total	306

Finally, we replace the L1-normalisation of the final BoVW features used in the DCF-BoVW method by L2-normalisation. Again, this allows us to exploit the property of cosine similarity in the SVM RBF kernel. Because BoVW features are sparse as many vector entries are zeros, cosine similarity is more appropriate than the Euclidean distance.

4. Experimental setup and comparison

4.1. Dataset

We use the COVID-19 dataset collected by [8] and [19]. It can be downloaded from the link ³. The dataset is the combination of chest x-ray images before COVID-19 and present chest x-ray images of COVID-19. This dataset consists of 306 chest x-ray images belonging to four categories (Covid, Normal, PneumoniaB, and PneumoniaV), each category contains at least 69 images. The number of images per class is listed in Table 1. The samples of one image per class from the dataset are shown in Fig. 4 In our experiment, we randomly divided the dataset into train and test at the ratio of 70/30 ratio per category and executed five runs and reported the average. Note that the results in all tables and line graphs are the average accuracies of five runs.

³COVID-19 Dataset Available online: <https://drive.google.com/uc?id=1coM7x3378f-Ou2l6Pg2wldaOI7Dntula> (accessed on Apr 17, 2020).

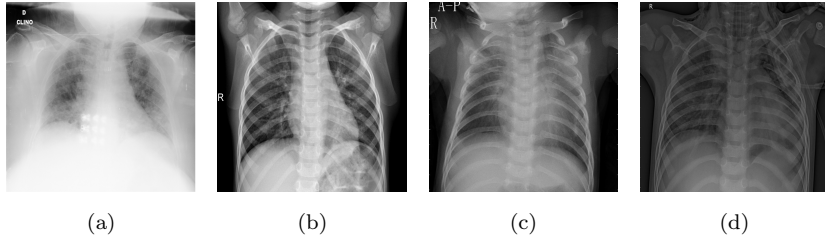


Figure 4: Example images from COVID-19 dataset for four classes: (a) Covid, (b) Normal, (c) PneumoniaB, and (d) PneumoniaV.

Table 2: Comparison of our method with existing methods on the testing set using features size and average classification accuracy (%).

Methods	Feat. size	Accuracy (%)
VGG16 (<i>GAP</i>) [37]	512-D	78.05
VGG19 (<i>GAP</i>) [37]	512-D	78.96
ResNet50 (<i>GAP</i>) [14]	2,048-D	79.48
DenseNet121 (<i>GAP</i>) [17]	1,024-D	76.12
Incep.-v3 (<i>GAP</i>) [47]	2,048-D	77.06
Incep.-Resv2 (<i>GAP</i>) [45]	1,536-D	75.90
Xception (<i>GAP</i>) [5]	2,048-D	75.69
DCF-BoVW [49]	400-D	72.46
Ours (VGG-16)	400-D	83.22

4.2. Implementation

To implement our work, we used Keras [6] implemented in Python [34]. Keras was used to implement the pre-trained model in our work. We used the number of clusters (k) in k -means clustering to define the dictionary to extract proposed features as 400. For the classification purpose, we used a support vector machine (SVM) classifier implemented using Scikit-learn [33] in Python. We normalized and standardized our features to feed into the SVM classifier. Moreover, we fixed the kernel as radial basis function (*RBF*) and γ parameter as $1e - 05$ in SVM. We automatically tuned the cost parameter C in the range of $\{1, 10, 20, \dots, 100\}$ on the training set using a 5-fold cross-validation method and used the optimal setting to train the model using the entire training set and tested on the test set. We executed all our experiments on a workstation with NVIDIA Geforce GTX 1080 Ti GPU and 128 GB RAM.

4.3. Comparison with the state-of-the-art methods

In this subsection, we present the results of the experiments conducted to compare our method with the state-of-the-art methods using *GAP* (global av-

Table 3: Comparison of our method with Loey et al. (2020)’s method based on the average classification accuracy (%). Note that we used Set 1 as designed by Loey et al. (2020) to compare with their methods.

Methods	Feat. size	Accuracy (%)
Loey et al. (2020) (AlexNet)	-	66.70
Loey et al. (2020) (GoogleNet)	-	80.60
Loey et al. (2020) (ResNet18)	-	66.70
Ours (VGG-16)	400-D	83.33

erage pooling) deep features extracted from several pre-trained models, DCF-BoVW and Loey et al. (2020)’s approach for the classification of COVID-19 chest x-ray images.

Pre-trained deep learning models could be one of the prominent features extractors for the classification purposes of images with limited data size as the Covid-19 dataset. We compared with *GAP* features extracted from the 4th layer of the VGG16 and VGG19 pre-trained models, and deep features extracted from the *avg_pool* layer of ResNet50, DenseNet121, Incep.-v3, Incep.-Resv2 and Xception pre-trained models. We also compared with the existing BoVW based features, DCF-BoVW, where the deep features from the 4th pooling layer of VGG16 were used with the same number of clusters ($k = 400$) as used in our experiment. The results of the comparison of our method with *GAP* deep features and DCF-BoVW are listed in Table 2.

Also, the comparative study results of our method with Loey et al. (2020)’s method are presented in Table 3. We used a separate table to present the results due to the varying train/test setup used by them. They used only one train-test split. We used exactly the same train-test split as them. In summary, to compare with Loey et al. (2020)’s method, we used their own setup, and to compare with remaining methods, we used our set up of five runs of 70/30 split.

From Table 2, we notice that our method performs better than the existing methods in terms of classification accuracy. Similarly, the size of the features of

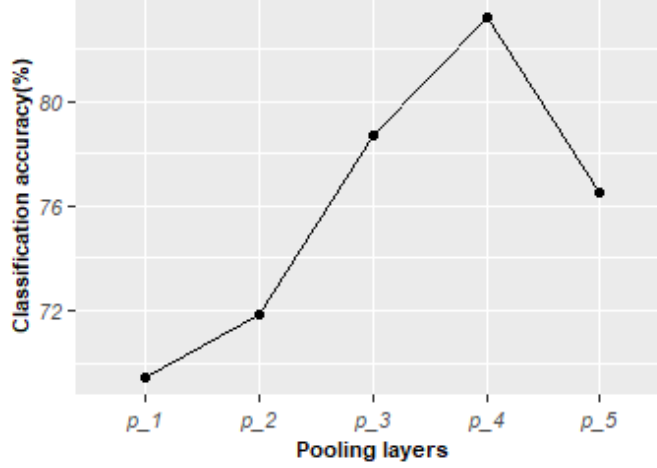


Figure 5: Average classification accuracy (%) achieved by our method using deep features extracted from the five pooling layers (p_1 to p_5) of the VGG16 model.

our method is lower than those of the existing methods. Similarly, from Table 3, we observe that our method based outperforms Loey et al. (2020)’s three methods. The stable classification accuracy along with lower features size of our method in both tables demonstrate the effectiveness of our method.

4.4. Ablative study of pooling layers

In this subsection, we present the results of an ablative study to analyze the effect on the classification accuracy of using deep features from the five different pooling layers of VGG16 in our method. The detailed results are presented in Fig. 5. While observing the line graph, we notice that the 4th pooling layer of the VGG16 model produces highly separable features than other pooling layers on the COVID-19 dataset.

4.5. Ablative study of cluster numbers

In this subsection, we analyze different unsupervised patterns to be used in our experiments. For this, we vary the cluster numbers from 100 to 500 ($\{100, 150, 200, \dots, 500\}$) and present the results in Fig. 6. From the line graph,

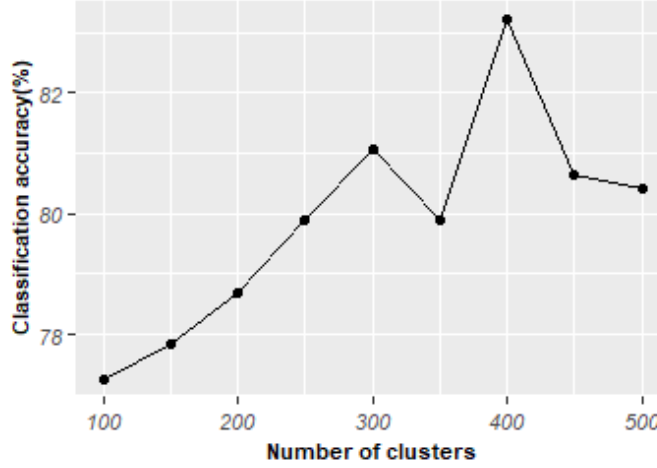


Figure 6: Average classification accuracy (%) with different cluster number. Note that deep features from the 4th pooling layer (p_4) were used.

we notice that the appropriate number of clusters that produce the best result is $k = 400$.

4.6. Ablative study of computation time

In this subsection, we study the computation time consumed in our method on the COVID-19 dataset and compare it with the time consumed by the second-best method in our experiment. We list the results in Table 4. From the table, we observe that the average features extraction and testing time per image (93 testing images) in our method are 0.16 seconds and 0.00008 seconds, respectively. This result shows that time consumption of our method is significantly lower than the second-best method’s (ResNet50(*GAP*)) time consumption in all three stages (features extraction, training, and testing).

4.7. Ablative study of class-wise performance

In this subsection, we study the average class-wise performance of our method. The average class-wise performance are reported using precision, recall, and f1-

Table 4: Average computation time (seconds) consumed by features extraction, training, and testing step in our method and the second best method (ResNet50(*GAP*)).

Method	Feat. extraction	Training	Testing
ResNet50(<i>GAP</i>) [14]	185.95	10.26	0.04
Ours	50.11	2.20	0.008

Table 5: Average class-wise study (%) over five runs of our method using precision, recall, and f1-score.

Class	Precision (%)	Recall (%)	F1-score (%)
Covid	100.00	97.20	98.40
Normal	94.20	93.60	93.80
PneumoniaB	75.80	67.60	71.00
PneumoniaV	68.00	76.80	71.80

score, which are defined in Eqs. (2),(3), and (4), respectively.

$$\text{Precision} = \frac{TP}{TP + FP}, \quad (2)$$

$$\text{Recall} = \frac{TP}{TP + FN}, \quad (3)$$

$$\text{F1-score} = \frac{2 \times (\text{Recall} \times \text{Precision})}{(\text{Recall} + \text{Precision})}, \quad (4)$$

where TP , FP , and FN represent true positive, false positive, and false negative, respectively. We present the average precision, recall, and f1-score in Table 5. The results show the discriminability of our proposed method in all four classes. It shows that our method can distinguish the Covid and normal class well and there is some confusion among two pneumonia classes.

5. Conclusion and future works

In this paper, we propose a new features extraction method based on Bag of Deep Visual Words (BoDVW) to represent chest x-ray images. Empirical results on the classification of chest x-ray images using the COVID-19 dataset show that our method is more appropriate to represent chest x-ray images. This is mainly because our features can capture a few interesting regions (sparse markers) indicating abnormalities well. Our features are extracted using a visual dictionary defined by the clustering of deep features from all training images. Therefore, they can capture patterns in each training image and thus helps to capture potential markers for various lung infections such as COVID-19 and pneumonia. Also, the size of our proposed features is relatively very small compared to other existing methods and our method runs faster than other existing methods.

Though the evaluation is done on a relatively small dataset, our method shows promising results to detect and distinguish lung infection due to pneumonia and COVID-19. COVID-19 being a relatively new disease and there are not a lot of chest x-ray images available. Nevertheless, given the current crisis with the COVID-19 pandemic, our method which is accurate and fast can be very useful for health professionals for mass screening of people for COVID-19. Accurate detection and distinction of lung infections due to COVID-19 and pneumonia are very important for COVID-19 diagnosis as people infected by these diseases show similar symptoms.

In the future, it would be interesting to verify our results in a large study with more sample images including other types of lungs infection such as tuberculosis. Another potential direction is to investigate if a similar approach can be used to represent other types of medical images such as CT scans, histopathological images, colonoscopy images, etc.

Acknowledgement

We would like to thank researchers, who spent their time to prepare such COVID-19 dataset in this difficult time.

References

- [1] N. S Altman. An introduction to kernel and nearest-neighbor nonparametric regression. *The American Statistician*, 46(3):175–185, 1992.
- [2] E. Ayan and H. M. Ünver. Diagnosis of pneumonia from chest x-ray images using deep learning. In *In Proc. Scientific Meeting on Electrical-Electronics & Biomedical Engineering and Computer Science (EBBT)*, pages 1–5, 2019.
- [3] A. Bastola, R. Sah, A. J Rodriguez-Morales, B. Kumar Lal, R. Jha, H. Chanda Ojha, B. Shrestha, D. KW Chu, L. LM Poon, A. Costello, et al. The first 2019 novel coronavirus case in nepal. *The Lancet Infectious Diseases*, 20(3):279–280, 2020.
- [4] L. Breiman. Random forests. *Machine learning*, 45(1):5–32, 2001.
- [5] F. Chollet. Xception: Deep learning with depthwise separable convolutions. In *Proc. IEEE Conf. Comput. Vis. Pattern Recognit.*, pages 1251–1258, 2017.
- [6] François Chollet et al. Keras. <https://github.com/fchollet/keras>, 2015.
- [7] V. Chouhan, S. Kumar Singh, A. Khamparia, D. Gupta, P. Tiwari, C. Moreira, R. Damaševičius, and V. H. C de Albuquerque. A novel transfer learning based approach for pneumonia detection in chest x-ray images. *Applied Sciences*, 10(2):559, 2020.
- [8] J. Paul Cohen, P. Morrison, and L. Dao. Covid-19 image data collection. *arXiv preprint arXiv:2003.11597*, 2020.

- [9] N. Dalal and B. Triggs. Histograms of oriented gradients for human detection. In *Proc. IEEE Comput. Soc. Conf. Comput. Vis. Pattern Recognit. (CVPR)*, pages 886–893, 2005.
- [10] J. Deng, W. Dong, R. Socher, L.-J. Li, K. Li, and L. Fei-Fei. ImageNet: a large-scale hierarchical image database. In *Proc. IEEE Conf. Comput. Vis. Pattern Recognit. (CVPR)*, 2009.
- [11] M. Giovanetti, D. Benvenuto, S. Angeletti, and M. Ciccozzi. The first two cases of 2019-ncov in italy: Where they come from? *Journal of medical virology*, 2020.
- [12] I. Goodfellow, J. Pouget-Abadie, M. Mirza, B. Xu, D. Warde-Farley, S. Ozair, A. Courville, and Y. Bengio. Generative adversarial nets. In *Proc. Advances in Neural Information Processing Systems*, pages 2672–2680, 2014.
- [13] Y. Guo, Y. Liu, S. Lao, E. M. Bakker, L. Bai, and M. S. Lew. Bag of surrogate parts feature for visual recognition. *IEEE Trans. Multimedia*, 20(6):1525–1536, Jun. 2018.
- [14] K. He, X. Zhang, S. Ren, and J. Sun. Deep residual learning for image recognition. In *Proc. IEEE Conf. on Computer Vision and Pattern Recognition (CVPR)*, pages 770–778, 2016.
- [15] M. A. Hearst. Support vector machines. *IEEE Intelligent Systems*, 13(4):18–28, 1998.
- [16] M. L Holshue, C. DeBolt, S. Lindquist, K. H Lofy, J. Wiesman, H. Bruce, C. Spitters, K. Ericson, S. Wilkerson, A. Tural, et al. First case of 2019 novel coronavirus in the united states. *New England Journal of Medicine*, 2020.
- [17] G. Huang, Z. Liu, L. Van Der Maaten, and K. Q. Weinberger. Densely connected convolutional networks. In *Proc. IEEE Conf. Comput. Vis. Pattern Recognit.*, pages 4700–4708, 2017.

- [18] S. R. Islam, S. P Maity, A. Kumar Ray, and M. Mandal. Automatic detection of pneumonia on compressed sensing images using deep learning. In *In Proc. Canadian Conference of Electrical and Computer Engineering (CCECE)*, pages 1–4, 2019.
- [19] D. S Kermany, M. Goldbaum, W. Cai, C. CS Valentim, H. Liang, S. L Baxter, A. McKeown, G. Yang, X. Wu, F. Yan, et al. Identifying medical diagnoses and treatable diseases by image-based deep learning. *Cell*, 172(5):1122–1131, 2018.
- [20] A. Krizhevsky, I. Sutskever, and G. E. Hinton. Imagenet classification with deep convolutional neural networks. In *Proc. Adv. Neural Inf. Process. Syst. (NIPS)*, pages 1097–1105, 2012.
- [21] A. Kumar, S. K. Singh, S. Saxena, K. Lakshmanan, A. K. Sangaiah, H. Chauhan, S. Shrivastava, and R. K. Singh. Deep feature learning for histopathological image classification of canine mammary tumors and human breast cancer. *Information Sciences*, 508:405–421, 2020.
- [22] C.-C. Lai, T.-P. Shih, W.-C. Ko, H.-J. Tang, and P.-R. Hsueh. Severe acute respiratory syndrome coronavirus 2 (sars-cov-2) and corona virus disease-2019 (covid-19): the epidemic and the challenges. *International Journal of Antimicrobial Agents*, page 105924, 2020.
- [23] S. Lazebnik, C. Schmid, and J. Ponce. Beyond bags of features: Spatial pyramid matching for recognizing natural scene categories. In *Proc. IEEE Comput. Soc. Conf. Comput. Vis. Pattern Recognit.*, pages 2169–2178, Jun. 2006.
- [24] D. D Lewis. Naive (bayes) at forty: The independence assumption in information retrieval. In *Proc. European Conference on Machine Learning*, pages 4–15, 1998.
- [25] C. Li, G. Zhu, X. Wu, and Y. Wang. False-positive reduction on lung

- nodules detection in chest radiographs by ensemble of convolutional neural networks. *IEEE Access*, 6:16060–16067, 2018.
- [26] J. Li, J. J. Li, X. Xie, X. Cai, J. Huang, X. Tian, and H. Zhu. Game consumption and the 2019 novel coronavirus. *The Lancet Infectious Diseases*, 20(3):275–276, 2020.
- [27] M. Loey, F. Smarandache, and N. E. M Khalifa. Within the lack of chest covid-19 x-ray dataset: a novel detection model based on gan and deep transfer learning. *Symmetry*, 12(4):651, 2020.
- [28] D. G Lowe. Distinctive image features from scale-invariant keypoints. *International Journal of Computer Vision*, 60(2):91–110, 2004.
- [29] L. Maaten and G. Hinton. Visualizing data using t-sne. *Journal of machine learning research*, 9(Nov):2579–2605, 2008.
- [30] A. Narin, C. Kaya, and Z. Pamuk. Automatic detection of coronavirus disease (covid-19) using x-ray images and deep convolutional neural networks. *arXiv preprint arXiv:2003.10849*, 2020.
- [31] A. Oliva. Gist of the scene. In *Neurobiology of Attention*, pages 251–256. Elsevier, 2005.
- [32] A. Oliva and A. Torralba. Modeling the shape of the scene: a holistic representation of the spatial envelope. *Int. J. Comput. Vis.*, 42(3):145–175, May. 2001.
- [33] F. Pedregosa, G. Varoquaux, A. Gramfort, V. Michel, B. Thirion, O. Grisel, M. Blondel, P. Prettenhofer, R. Weiss, V. Dubourg, et al. Scikit-learn: Machine learning in python. *the Journal of machine Learning research*, 12:2825–2830, 2011.
- [34] G. Rossum. Python reference manual. Technical report, Amsterdam, The Netherlands, 1995.

- [35] T. Sasaki, K. Kinoshita, S. Kishida, Y. Hirata, and S. Yamada. Ensemble learning in systems of neural networks for detection of abnormal shadows from x-ray images of lungs. *Journal of Signal Processing*, 16(4):343–346, 2012.
- [36] J. M Sharfstein, S. J Becker, and M. M Mello. Diagnostic testing for the novel coronavirus. *Jama*, 2020.
- [37] K. Simonyan and A. Zisserman. Very deep convolutional networks for large-scale image recognition. *arXiv preprint arXiv:1409.1556*, 2014.
- [38] T. Singhal. A review of coronavirus disease-2019 (covid-19). *The Indian Journal of Pediatrics*, pages 1–6, 2020.
- [39] C. Sitaula and S. Aryal. Fusion of whole and part features for the classification of histopathological image of breast tissue. *Health Information Science and Systems*, 8(1):1–12, 2020.
- [40] C. Sitaula, S. Aryal, Y. Xiang, A. Basnet, and X. Lu. Content and context features for scene image representation. *arXiv preprint arXiv:2006.03217*, 2020.
- [41] C. Sitaula and MB Hossain. Attention-based vgg-16 model for covid-19 chest x-ray image classification. *Applied Intelligence*, pages 1–14, 2020.
- [42] C. Sitaula, Y. Xiang, S. Aryal, and X. Lu. Scene image representation by foreground, background and hybrid features. *arXiv preprint arXiv:2006.03199*, 2020.
- [43] C. Sitaula, Y. Xiang, A. Basnet, S. Aryal, and X. Lu. Hdf: Hybrid deep features for scene image representation. *arXiv preprint arXiv:2003.09773*, 2020.
- [44] O. Stephen, M. Sain, U. J. Maduh, and D.-U. Jeong. An efficient deep learning approach to pneumonia classification in healthcare. *Journal of healthcare engineering*, 2019, 2019.

- [45] C. Szegedy, S. Ioffe, V. Vanhoucke, and A. A. Alemi. Inception-v4, inception-resnet and the impact of residual connections on learning. In *Proc. Thirty-first AAAI conference on artificial intelligence*, 2017.
- [46] C. Szegedy, W. Liu, Y. Jia, P. Sermanet, S. Reed, D. Anguelov, D. Erhan, V. Vanhoucke, and A. Rabinovich. Going deeper with convolutions. In *Proc. IEEE Conf. Comput. Vis. Pattern Recognit. (CVPR)*, pages 1–9, Jun. 2015.
- [47] C. Szegedy, V. Vanhoucke, S. Ioffe, J. Shlens, and Z. Wojna. Rethinking the inception architecture for computer vision. In *Proc. IEEE Conf. Comput. Vis. Pattern Recognit.*, pages 2818–2826, Jun. 2016.
- [48] D. Varshni, K. Thakral, L. Agarwal, R. Nijhawan, and A. Mittal. Pneumonia detection using cnn based feature extraction. In *In Proc. International Conference on Electrical, Computer and Communication Technologies (ICECCT)*, pages 1–7, 2019.
- [49] J. Wan, A. Yilmaz, and L. Yan. Dcf-bow: Build match graph using bag of deep convolutional features for structure from motion. *IEEE Geoscience and Remote Sensing Letters*, 15(12):1847–1851, 2018.
- [50] B. Zhou, A. Khosla, A. Lapedriza, A. Torralba, and A. Oliva. Places: An image database for deep scene understanding. *arXiv preprint arXiv:1610.02055*, 2016.
- [51] Z.-H. Zhou, Y. Jiang, Y.-B. Yang, and S.-F. Chen. Lung cancer cell identification based on artificial neural network ensembles. *Artificial Intelligence in Medicine*, 24(1):25–36, 2002.